In Vivo Targeted Cancer Imaging, Sentinel Lymph Node Mapping and Multi-Channel Imaging with Biocompatible Silicon Nanocrystals

Folarin Erogbogbo,[†] Ken-Tye Yong,[‡] Indrajit Roy,[‡] Rui Hu,[‡] Wing-Cheung Law,[‡] Weiwei Zhao,[‡] Hong Ding,[‡] Fang Wu,[‡] Rajiv Kumar,[‡] Mark T. Swihart,[†,‡,*] and Paras N. Prasad[‡,§,*]

[†]Department of Chemical and Biological Engineering, [§]Department of Chemistry, and [‡]Institute for Lasers, Photonics and Biophotonics, University at Buffalo (SUNY), Buffalo, New York 14260-4200, United States

ABSTRACT Quantum dots (QDs) have size-dependent optical properties that make them uniquely advantageous for *in vivo* targeted fluorescence imaging, traceable delivery, and therapy. The use of group II—VI (e.g., CdSe) QDs for these applications is advancing rapidly. However, group II—VI QDs contain toxic heavy metals that limit their *in vivo* applications. Thus, replacing these with QDs of a biocompatible semiconductor, such as silicon (Si), is desirable. Here, we demonstrate that properly encapsulated biocompatible Si QDs can be used in multiple cancer-related *in vivo* applications, including tumor vasculature targeting, sentinel lymph node mapping, and multicolor NIR imaging in live mice. This work overcomes dispersibility and functionalization challenges to *in vivo* imaging with Si QDs through a unique nanoparticle synthesis, surface functionalization, PEGylated micelle encapsulation, and bioconjugation process that produces bright, targeted nanospheres with stable luminescence and long (>40 h) tumor accumulation time *in vivo*. Upon the basis of this demonstration, we anticipate that Si QDs can play an important role in more sophisticated *in vivo* models, by alleviating QD toxicity concerns while maintaining the key advantages of QD-based imaging methods.

KEYWORDS: silicon quantum dots · tumor targeting · sentinel lymph node mapping · multiplex imaging · near-infrared

Quantum dots (QDs) for *in vivo* fluorescence imaging have generated intense interest due to their high brightness, photostability, and broad excitation spectrum.[1,2] QDs are semiconductor nanocrystals with electronic and optical properties that depend on their size, shape, composition, and surface coating.[3,4] In general, QDs with a core/shell structure are preferable for biomedical applications.[5] The core is commonly composed of elements from groups II and VI (e.g., CdSe) or III and V (e.g., InP) of the periodic table.[5,6] Targeted *in vivo* imaging of tumors with Cd-based QDs has been demonstrated in small animals.[6] However, Cd is toxic at low concentrations,[7] and release of free metal ions is a significant concern.[8,9] The cytotoxicity of these QDs is reduced when their cores are protected by biocompatible coatings. However, some recent reports suggest that cadmium ion release remains a major concern.[10] Therefore, new heavy-metal-free QDs are needed, particularly for *in vivo* applications. Bawendi's group has synthesized near-infrared (NIR) emitting core/shell/shell $InAs_xP_{1-x}$/InP/ZnSe QDs and used them in sentinel lymph node (SLN) mapping studies.[11] Pons *et al.*[12] used CuInS/ZnS for SLN mapping and showed decreased toxicity compared to cadmium-based QDs. Although these QDs are cadmium-free, they do contain other heavy metals.

Luminescent Si nanocrystals have potential applications ranging from electronics to medicine.[13−29] Several methods of synthesizing Si QDs,[15,17] including etching of porous Si,[29] laser ablation,[25,28] and solution-phase methods[22−24] have been reported. However, these generally produce small (submilligram) quantities of high-quality Si nanocrystals. More recent approaches including low-pressure plasma synthesis[27] and thermal processing of silesquioxanes[26] can produce larger quantities but remain less convenient than solution-phase approaches used for II−VI quantum dots. Si QDs with size-dependent luminescence spanning the visible spectrum have not been prepared by solution-phase approaches, and this has hampered their development.

We have developed a unique two-step method based on laser pyrolysis of silane, followed by acid etching, to produce Si QDs with high quantum yield (QY) and size-tunable emission at wavelengths from 450 to over 800 nm.[14,30] We functionalize these

*Address correspondence to pnprasad@buffalo.edu, swihart@buffalo.edu.

Received for review August 3, 2010 and accepted November 23, 2010.

Published online December 7, 2010. 10.1021/nn1018945

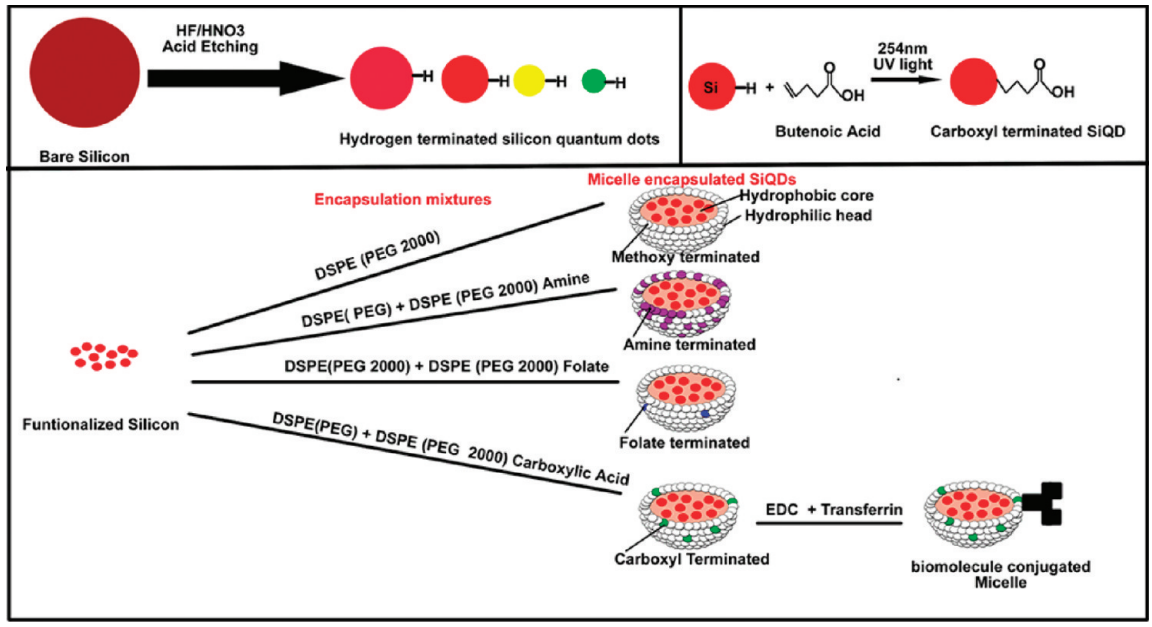

Scheme 1. Synthesis and Surface Functionalization of Si Quantum Dots

with organic molecules to obtain colloidally stable dispersions. QYs as high as 70% have been reported for Si QDs emitting in the NIR,[31] but QY at shorter wavelengths is lower. Si QDs can provide many of the advantages of other QDs without the toxicity concerns that plague heavy metal based QDs. Si QDs also maintain their optical properties under two and three photon excitation in polar and nonpolar solvents.[32] These advantages, along with the abundance and low cost of Si, make Si QDs an attractive candidate to complement or replace heavy-metal-based QDs in various applications.

Unlike components of group II−VI and IV−VI QDs (including Cd, Pb, Hg, Se, and Te), Si is nontoxic in its elemental form. Bulk and porous Si exhibit minimal toxicity, and this can be expected to hold for Si nanocrystals as well. Canham even proposed nanoscale Si as a food additive.[33] Si-QDs were claimed to be at least 10 times safer than Cd-based QDs under UV irradiation.[34] Exposed elemental Si is expected to be metabolized to silicic acid, which is readily cleared by the kidneys.[35,36] Sailor's group recently demonstrated that dextran-modified biodegradable porous silicon can be used for enhanced permeation and retention (EPR) based tumor targeting and *in vitro* chemotherapeutic drug delivery.[36] These nontargeted porous, luminescent constructs are promising carriers for traceable drug delivery, but provide less flexibility for other applications compared to the free-standing Si QDs formulations presented here. Conventional QDs have shown promise in applications such as sentinel lymph node (SLN) mapping,[37] tumor targeting,[6,38] and multiplex imaging.[39] Here, we create rationally designed Si QD-based probes (Scheme 1) that avoid enzymatic degradation, evade uptake by the reticuloendothelial system (RES), maintain stability in the acidic tumor microenvironment, and produce bright and stable photoluminescence *in vivo*. These features, along with low toxicity, are essential to their ultimate clinical applicability for cancer applications such as tumor visualization, traceable drug delivery, and SLN mapping.

A key obstacle to applying Si QDs in bioimaging has been their oxidative degradation in the biological environment. We have overcome this through surface functionalization and PEGylated micelle encapsulation of Si QDs. Here, we provide the first demonstrations of *in vivo* tumor targeting, SLN mapping, and multiplex imaging using free-standing Si QDs. Moreover, although toxicity of bulk and porous silicon have been studied and a few studies of SiQDs have demonstrated their low cytotoxicity,[40−42] Si QDs modified for cancer applications have not been evaluated. Thus, we assessed *in vivo* cytotoxicity of the micelle encapsulated Si QDs in mice, along with *in vitro* cytotoxicity for Si QDs of varied particle size, surface functionalization, and encapsulation.

RESULTS AND DISCUSSION

Nanoparticle Synthesis and Characterization. Scheme 1 illustrates the synthesis and surface functionalization of water dispersible Si QDs using photoinitiated hydrosilylation and micelle-encapsulation. Three types of Si QDs were used in this study: (1) hydrogen-terminated Si QDs; (2) carboxyl-terminated Si QDs created by reacting butenoic acid with the H-terminated Si QDs; and (3) Si particles encapsulated in phospholipid micelles using DSPE-PEG(2000). DSPE-PEG(2000) refers to 1,2-distearoyl-sn-glycero-3-phosphoethanolamine-*N*-[methoxy (polyethylene glycol)-2000] (ammonium salt) and DSPE-PEG(2000) Amine refers to 1,2-distearoyl-sn-glycero-3-phosphoethanolamine-*N*-

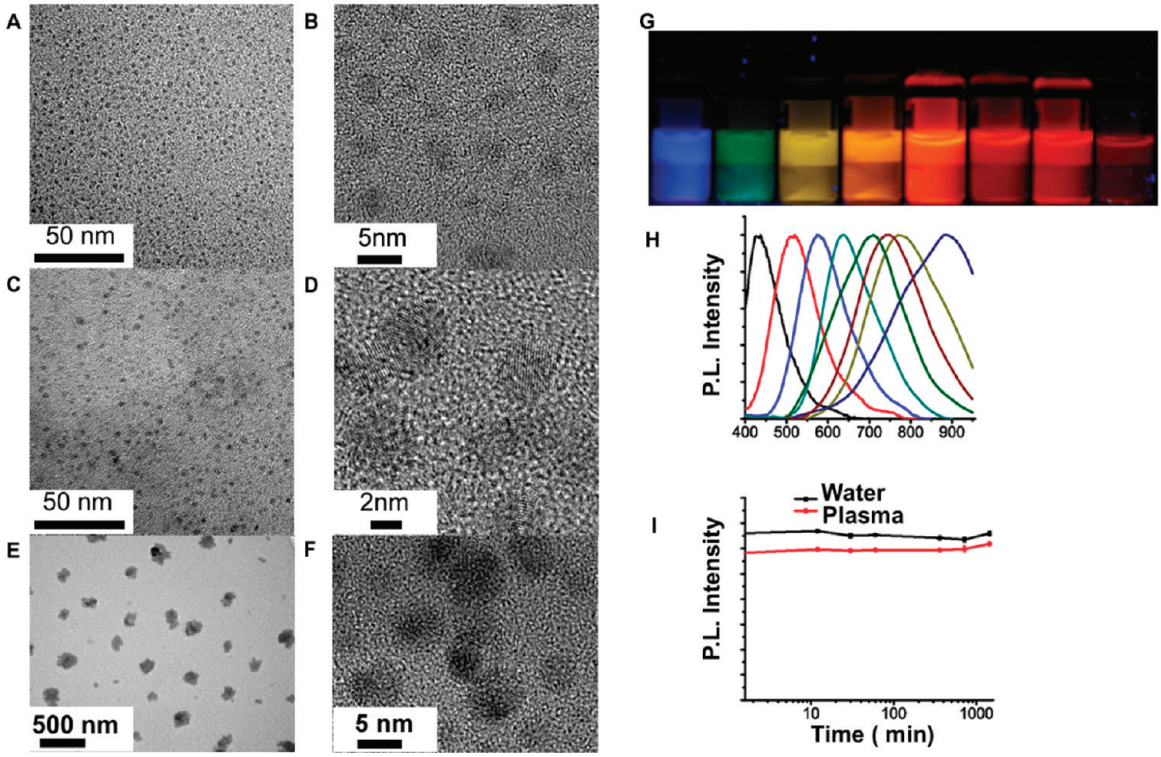

Figure 1. Characterization of visible and NIR emitting Si QDs produced by etching of laser-synthesized Si nanoparticles. (A−F) Transmission Electron Microscope (TEM) images of (A,B) green-emitting Si QDs, (C,D) orange-emitting Si QDs, (E,F)formaldehyde fixed micelle encapsulated Si QDs, (G) photograph of Vis-NIR-emitting Si QDs excited by a single source (365 nm). (H) Normalized emission spectra from Visible-NIR Si-QDs, and (I) spectral stability of luminescent Si particles in water and plasma.

[amino(polyethylene glycol)-2000] (ammonium salt). Replacing the word amine in the name above with carboxyl or folate gives the corresponding name in Scheme 1 Octadecene, ethyl undecylenate, and styrene functionalized Si QDs were used for encapsulation. Overall, unetched Si nanoparticles, etched Si particles, carboxyl-terminated nanocrystals, micelle-encapsulated nanocrystals with positive, negative and neutral charges, and bioconjugated micelle-encapsulated Si QDs were prepared. PEGylated micelle-encapsulated QDs were used in the *in vivo* imaging and toxicity studies.

Visible and NIR emitting Si QDs (Figure 1G,H) were produced by etching of laser-synthesized Si nanoparticles[43,44] followed by covalent linking of organic ligands to their surfaces using photoinitiated hydrosilylation.[14] Transmission Electron Microscopy (TEM) of these showed quasi-spherical particles from 2 to 8 nm in diameter (Figure 1A,B,C,D). Lattice fringes were observed, demonstrating that even these small particles are crystalline. Parts C through F of Figure 1 show ethyl undecylenate-grafted Si QDs before and after encapsulation. When stored at 4 °C, the optical properties of these dispersions in HPLC water remained stable for at least 6 months; no aggregation or degradation of photoluminescence was observed. TEM of formaldehyde-fixed micelle-encapsulated Si QDs showed spherical aggregates of crystalline particles with 50 to 120 nm overall diameter (Figure 1E,F). The hydrodynamic diameter measured by dynamic light scattering (DLS) was 60 to 160 nm (Figure S1A, Supporting Information). Multiple Si QDs are encapsulated in each micelle, in contrast to the more common encapsulation of single QDs. The hydrodynamic diameter increased slightly upon linking of RGD peptide to the surface for tumor targeting (Figure S1B, Supporting Information). Smaller micelles were prepared for SLN mapping (Figure S1C, Supporting Information).

As shown in Figure 1H, the Si QD photoluminescence (PL) emission red-shifts from ~450 to ~900 nm with increasing particle size. The particles sizes range from 2 to 8 nm as they change from green to NIR emitting particles. Narrower PL spectra can be obtained by fractionating the samples.[5] Absorbance spectra are shown in Figure S2. The typical QY was ~5−10% after micelle encapsulation, which is sufficient for bioimaging (Figure S4, Supporting Information). PL was stable to changes in pH and temperature,[45] and under UV illumination, and did not show any significant change in photoluminescence intensity after one to two months of storage at 4 °C. Results of *in vitro* cytotoxicity assays are available in the Supporting Information (Figure S3, S5). No aggregation or significant change in size were observed in particles suspended cell culture media or plasma.

Based on the importance of NIR emission for *in vivo* applications,[37,38] Si QDs with peak emission at 700−800 nm were used for SLN mapping and tumor targeting.

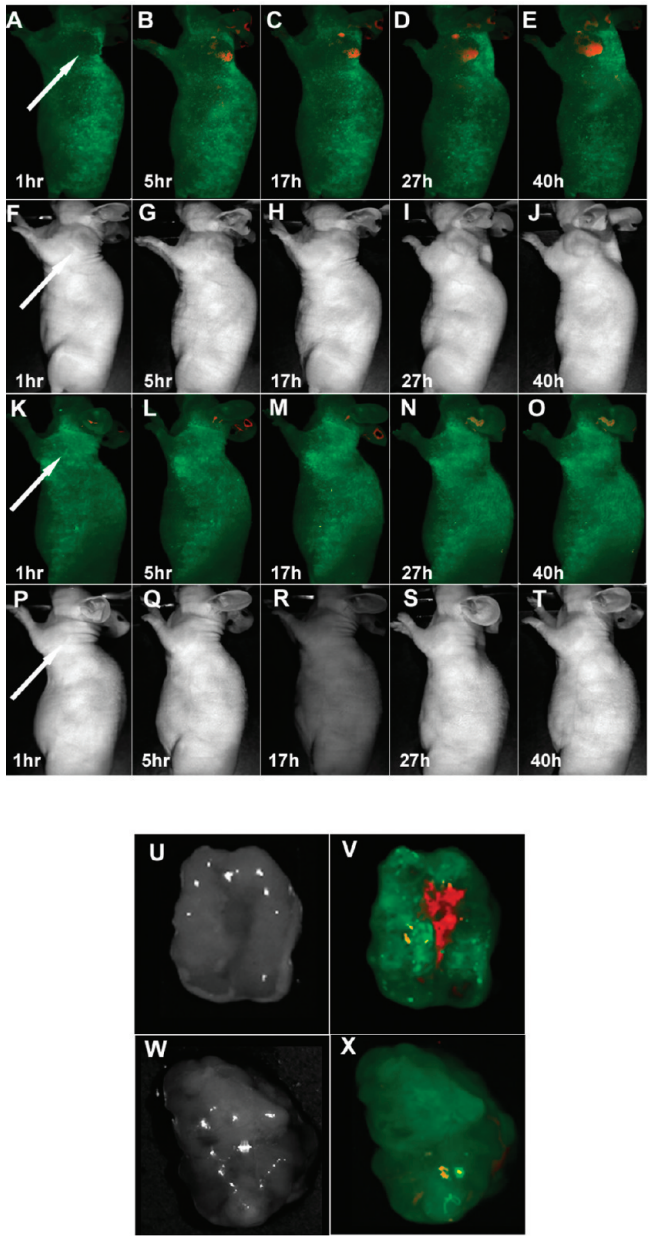

Figure 2. Time-dependent *in vivo* luminescence imaging of Panc-1 tumor bearing mice (left shoulder, indicated by white arrows) injected with ~5 mg of (A−E) MSiQD-RGD or (K−O) MSiQD. All images were acquired under the same conditions. Autofluorescence and the unmixed SiQD signal are coded in green and red, respectively. Panels F−J and panels P−T correspond to the luminescence images in panels A−E and K−O, respectively. *Ex vivo* images (U,W) and luminescence images (V,X) of tumors harvested at 40 h postinjection from mice treated with (U,V) MSiQD-cRGD or (W,X) MSiQD.

Intimate contact with blood makes the tumor endothelial cell a uniquely accessible target within the tumor, and we take advantage of this in our design of bioconjugated Si QDs. Based on prior demonstrations of targeting of $\alpha_v\beta_3$ integrins that are overexpressed in the tumor vasculature,[38] micelle encapsulated Si QDs were conjugated to RGD peptides that bind to $\alpha_v\beta_3$ integrins for tumor targeting. We refer to these as MSiQD-RGD.

***In vivo* Tumor Targeting.** Nude mice bearing subcutaneously implanted Panc1-tumors (4 weeks post inoculation of 2 to 4 × 10^6 cells on left shoulder, tumor volume of 0.5−0.9 cm^3) were intravenously injected with MSiQD-RGD (380 mg/kg, ~2 nmol of RGD peptide, *via* tail vein). Luminescence imaging was performed at multiple time points post injection (p.i) using the Maestro *in vivo* imaging system (CRI, Inc., Woborn, MA; excitation 445−490 nm, emission: 645 nm long pass). Wavelength resolved spectral unmixing confirmed the presence of NIR emission from Si QDs targeted to the tumor vasculature. The luminescence intensity at the tumor site increased with time up to 40 h p.i. (Figure 2A−E). This demonstrated the effectiveness of tumor targeting using MSiQD-RGD and also that the accumulation time of the MSiQD-RGD was at least 40 h. The observed accumulation time was significantly longer (~8−10 times) than that observed in previous reports,[6,38] in which smaller single CdSe and CdTe-based QDs were used. Detailed circulation studies are beyond the scope of the work, however the accumulation time implies that circulation times may be comparably long. Nonbioconjugated MSiQDs with the same PEG coating were intravenously injected into tumor-bearing mice, and no uptake of the particles was observed in the tumors (Figure 2K−O).

The tumors were resected and imaged immediately after sacrificing the mice (40 h p.i.). As shown in Figure 2U−X, the QD signal is more visible in the resected Panc-1 tumor of the mouse injected with the MSiQD-RGD formulation (Figure 2V). Although the QD signal is not clearly visible in the tumors of mice injected with the nonbioconjugated MSiQD formulation, careful analysis shows that a small amount of luminescence is present (Figure 2X). Detailed signal intensity analysis showed that the total SiQD luminescence intensity from the MSiQD-cRGD tumor was 186 times that from the MSiQD tumor. The small MSiQD *ex vivo* luminescence signal is attributed to the enhanced permeation and retention (EPR) effect, while the much larger signal from the MSiQD-cRGD clearly demonstrates targeted uptake. Biodistribution studies were also performed, and uptake of the particles was observed in the liver and spleen as well as the tumor. The uptake in the liver and spleen was reduced for the targeted particles, compared to the untargeted ones (Figure S6). The RES uptake of nanomaterials is known to be size dependent, and the observed biodistribution of the Si QDs is similar to that of other nanomaterials (sizes ~10−150 nm) that tend to undergo RES uptake, particularly in the liver and spleen.[6,38]

Sentinel Lymph Node Mapping. One of the most promising cancer-related applications of QDs is SLN mapping. Group II−VI NIR QDs have been used for SLN mapping because of their potential to eliminate the use of both a radioactive tracer and a blue dye. They provide surgical image guidance that allows high sensitivity surgical site inspection, identification of SLN after resection, and elimination of marker flow past the lymph node.[37,46] Fig-

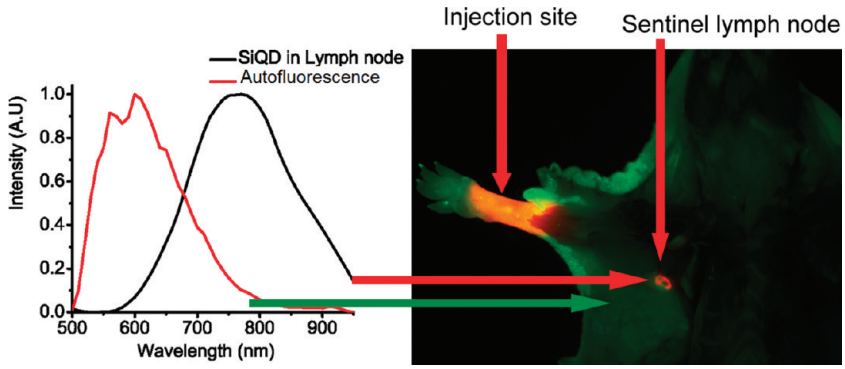

Figure 3. Sentinel lymph node imaging following localization of Si QDs in an axillary position. Autofluorescence is coded in green, and the unmixed SiQD signal is coded in red

ure 3 demonstrates application of nontargeted MSiQDs with hydrodynamic radii as small as 20 nm that were tailored for the same purpose. When injected subcutaneously in the paw of a mouse ($n = 3$), MSiQDs traveled through the lymphatics and migrated to an axillary location that could be detected using the Maestro imaging system. The localization of MSiQD indicates the position of the SLN. Though improvements remain to be made, this demonstration, along with demonstration of multiphoton excitation of the NIR (windows of 700−900 and 1200−1600) Si QDs,[47] and reports of Si QD QY in the NIR above 60%,[31] suggest that Si QDs are worthy of serious further consideration as replacements for traditional tracers used in SLN mapping. CuInS/ZnS quantum dots have also been considered heavy metal-free quantum dots with great potential in this application,[12] however they still contain metals that may cause some concern.

***In vivo* Multicolor Imaging.** Absorption and autoluminescence from tissues reach minima in the NIR region, which provides a clear window for *in vivo* optical imaging.[38] With II−VI materials, NIR emission has required more complex QDs (e.g., $CdSe_xTe_{1-x}$). This leads to mixing of immunostimulatory components, exacerbating toxicity concerns. This is overcome by SiQDs because their emission extends beyond 900 nm without changes in composition. At least four distinguishable peaks can be observed from the far red to the NIR (Figure 1H). Most of the methods used to produce SiQDs do not produce particles that emit in the NIR; therefore it is important to show demonstrations of those that do. Figure 4 demonstrates that NIR peaks can easily be distinguished *in vivo* after subcutaneous injection of MSiQDS fabricated using a 1:20 silicon to phospholipid (w/w) ratio. Luminescence from QDs at different spots can be easily separated from the autofluorescence and from one another. This provides a demonstration that the micelle-encapsulated Si QDs can be used as biocompatible NIR multicolored optical probes for *in vivo* multiplex imaging.

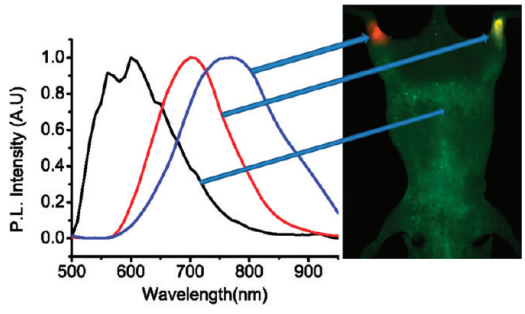

Figure 4. *In vivo* multiplex NIR imaging of Si QDs subcutaneously injected in lower limbs of a mouse. Autofluorescence and unmixed SiQD signals are coded in green, red and yellow, as indicated by associated unmixed spectra.

***In vivo* Toxicity.** Nonbioconjugated micelle-encapsulated Si QDs were intravenously injected into healthy mice to study *in vivo* distribution, clearance, and toxicity. The body weight of the untreated (saline-injected) and treated (MSiQD-injected) mice as a function of time is shown in Figure 5. No significant changes in body weight were observed for more than four weeks postinjection, and no changes in eating, drinking, exploratory behavior, activity, or physical features (e.g., hair, color) were observed. This strongly suggests that the MSiQD formulation is nontoxic *in vivo* at this dosage of ~380 mg/kg, which corresponds to about 60 nmol of Si QDs per mouse, roughly 10 times higher than the highest dose of CdSe/ZnSe QDs used by Gao and Nie in their *in vivo* tumor imaging studies.[6] This suggests that Si QDs can be safely applied at much higher dosages than Cd-based QDs. Further studies at even higher MSiQD dosages will be required to determine their maximum tolerable dosage (MTD).

Figure 6 shows the biodistribution of MSiQDs in a healthy mouse sacrificed 24 h post injection. Luminescence from the Si QDs indicates that they localize in the liver and spleen. In tumored nude mice with compromised immune systems, the uptake was more prominent in the liver than in the spleen (Figure S6, Supporting Information). In BALB/c mice without compromised immune systems, the average signal was higher in the spleen than the liver (Figure 6). The overall luminescence signal decreases as a function of time indicating that the MSiQDs are degraded in the liver and the spleen. The luminescence completely disappeared from the liver and decreased by about 95% in the spleen af-

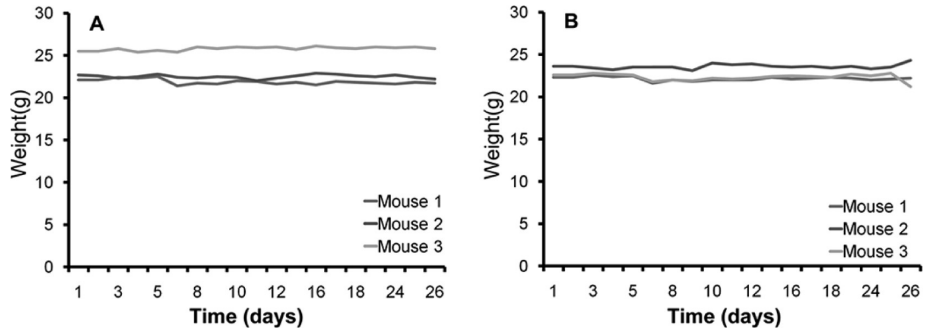

Figure 5. Evolution of mouse body weight following injection of (A) MSiQDs or (B) saline only.

ter two months (Figure S7, Supporting Information). Figure 7 shows histology results for tissues (lung, heart, spleen, kidney, and liver), comparing the effects of PBS and micelle-encapsulated Si QDs on the treated mice. No pathological changes or signs of overt toxicity (tissue degeneration or necrosis) were observed, further confirming the nontoxicity and biocompatibility of micelle-encapsulated Si QDs.

Serum analysis was also used to evaluate *in vivo* toxicity of the MSiQDs at two months postinjection. Blood samples were collected and immediately sent for blood analysis (BioReliance, www.bioreliance.com) to assess AST (aspartate aminotransferase), ALT (alanine aminotransferase), ALP (alkaline phosphatase), TBILI (total bilirubin), GLU (glucose), TPROT (total protein serum), CREAT (creatinine), BUN (blood urea nitrogen) and ALB (albumin) levels. These indicators are commonly used to evaluate kidney, renal and hepatic functions. All serum levels were within the normal ranges as depicted in Table 1. These results confirm that there are no ad-

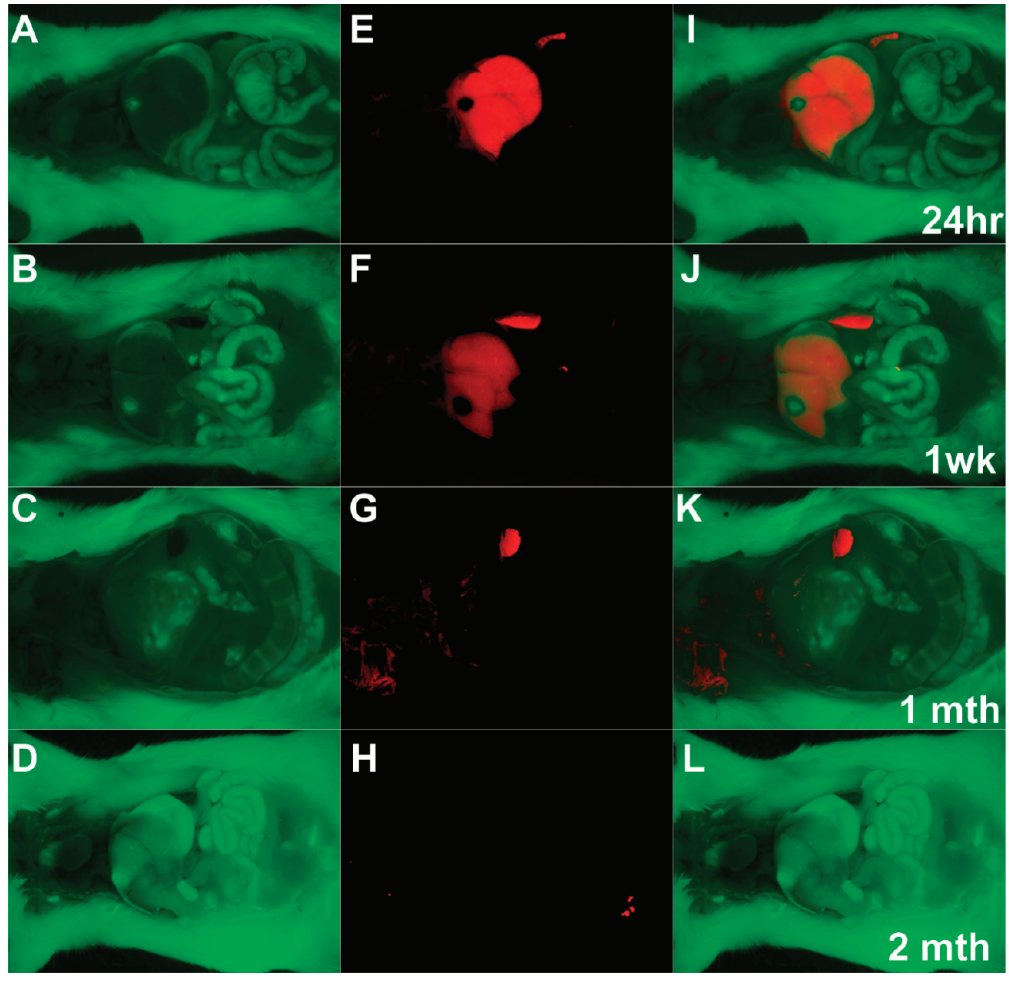

Figure 6. Luminescence imaging of BALB/c mice injected with MSiQD. All images were acquired at the same instrument settings, at different time points postinjection. Autofluorescence is shown in green (left panels) and the QD signal is shown in red (center panels). The right panels show overlaid autofluorescence and QDs luminescence images. Uptake in the liver and spleen was observed.

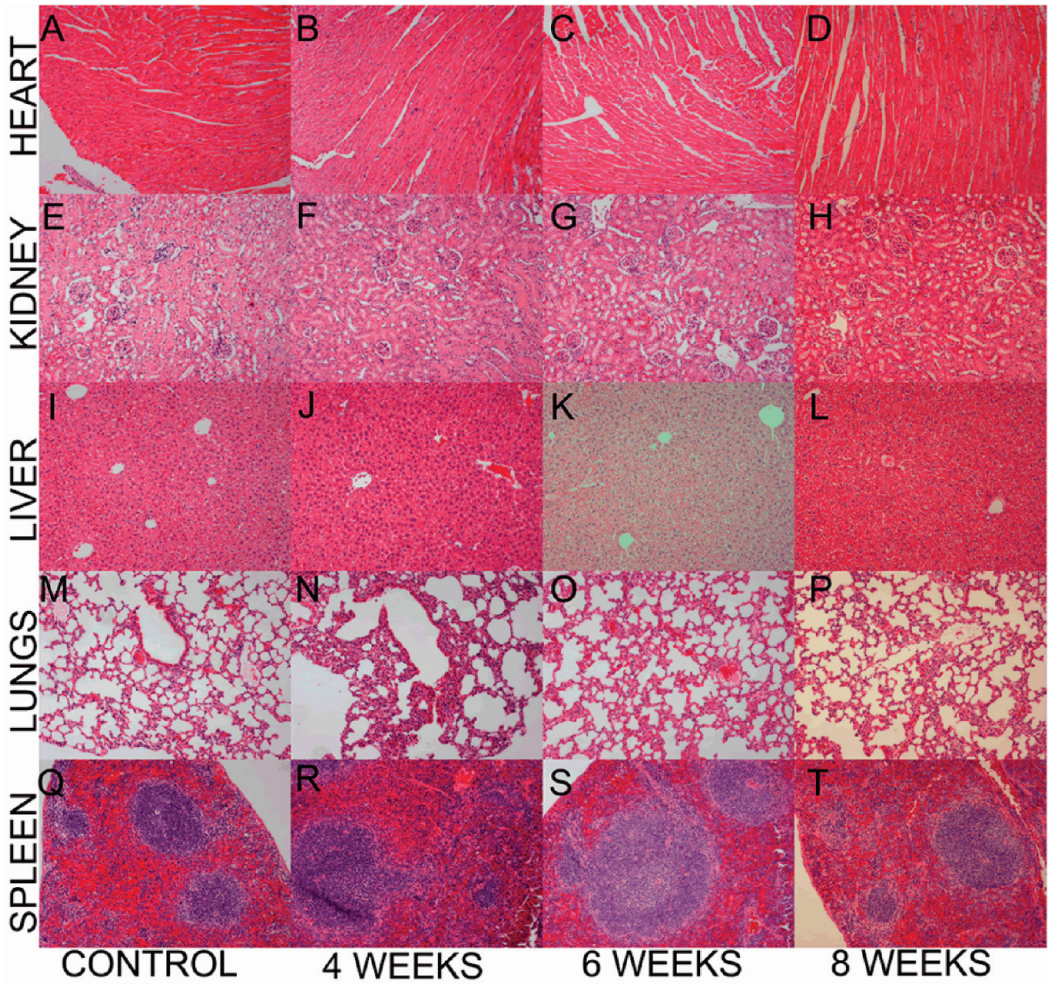

Figure 7. Histopathology images of the (A−D) heart, (E−H) kidney, (I−L) liver, (M−P) lungs, and (Q−T) spleen. Mice were treated with ~380 mg/kg of micelle-encapsulated QDs (approximately 60 nmol Si QDs per mouse) and sacrificed at 4 weeks (column 2), 6 weeks (column 3), and 8 weeks (column 4). The control mouse (column 1) was treated with saline only and sacrified 24 h post injection. All images are at identical magnification.

verse effects in small animals from injection of MSiQD at 380 mg per kg.

***In vitro* Cytotoxicity Comparison with Cd-based QDs.** To compare cytotoxicity between NIR-emitting cadmium-based and Si QDs, two types of cadmium based QDs were prepared, namely, CdTe and CdHgTe QDs, both functionalized with L-cysteine, for comparison to Si QDs terminated with butenoic acid. This provides both types of QDs with similar carboxylic acid surface termination. Figure 8 shows the *in vitro* cytotoxicity assay results for Si, CdTe and CdHgTe QDs on a human pancreatic cancer (Panc-1) cell line at 24 h post-treatment. The inhibitory particle concentrations corresponding to 50% cell viability (IC_{50}) were 20 μg/mL and 11 μg/mL for CdTe and CdHgTe in Panc-1 cells, respectively, compared to >500 μg/mL for Si.

DISCUSSION

In recent reports, no adverse effects were found in mice treated with micelle-encapsulated CdSe QDs over a short period of time. However, Cd-based QDs may still degrade in the biological environment and cause acute toxicity. Nie's group,[10] has suggested that if it is revealed in the near future that Cd ions are indeed released in the biological environment, then new types of QDs must be developed for advancing QD-based bioimaging. The ultimate objective of our development of Si QDs for bioapplications is to enable imaging, target-

TABLE 1. Comparison of Serum AST, ALT, ALP, TBILI, GLU, TPROT, CREAT, BUN, and ALB between Treated Mice ($N = 3$) and the Normal Range

	AST (UL^{-1})	ALT (UL^{-1})	ALP (UL^{-1})	TBILI ($mg\ dL^{-1}$)	GLU ($mg\ dL^{-1}$)	TPROT ($g\ dL^{-1}$)	CREAT ($mg\ dL^{-1}$)	BUN ($mg\ dL^{-1}$)	ALB ($g\ dL^{-1}$)
Results	137 ± 11	25 ± 16	70 ± 12.	0.45 ± 0.2	178 ± 36	4.7 ± 0.5	0.41 ± 0.07	16.5 ± 2.1	2.85 ± 0.3
Normal Range	52−298	17−77	35−222	0.0−0.9	140−263	3.9−6.4	0.2−0.90	9−22	2.5−4.6

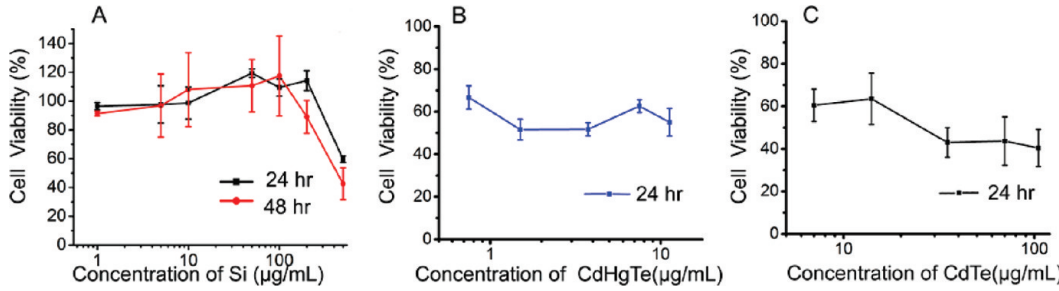

Figure 8. Cytotoxicity of (A) Si, (B) CdTe, and (C) HgCdTe quantum dots toward Panc-1 cells. Error bars represent standard deviation ($N = 3$). Note that the concentration range is much higher in (A) than in (B) and (C).

ing and treatment of neoplastic sites. To the best of our knowledge, these are the first successful demonstrations of *in vivo* targeted tumor imaging and SLN mapping using discrete Si QDs, as opposed to porous silicon constructs, as well as the first time 4 NIR peaks from Si QDs have been distinguished. The similarity of between porous and discrete silicon lies in their possible degradation routes, and in the low toxicity of the core material, as demonstrated by Park *et al.*[36] However, porous silicon and the free-standing silicon nanoparticles are significantly different in many ways including surface chemistry, structure, and luminescence properties. These differences are substantial enough that they may be considered completely different nanostructures. Confining Si QDs in the oil-like interior of a phospholipid-PEG micelle protects them from rapid degradation, and enhances their long-term blood circulation. Degradation induced toxicity is not a significant concern with Si QDs, in sharp contrast to Cd based QDs. For Si QDs, agglomeration and spectral instability are more important issues, and micelle encapsulation addresses both. In addition, the presence of suitable functional groups on the surface of micelles can be used for conjugation with desired biomolecules for target-specific delivery. The PEG coating reduces uptake into the RES and thereby increases the circulation time for localization in cancerous sites. Ducongé *et al.* demonstrated long circulation times of quantum dots on the order of 2 h.[48]

This work demonstrates that Si QDs can be used as biocompatible fluorescent probes for both *in vitro* and *in vivo* imaging, including multicolor imaging at NIR wavelengths. Both *in vitro* and *in vivo* experiments showed that these particles could be safely used at high doses with minimal cytotoxicity. *In vitro* cytotoxicity assays showed minimal toxicity from a variety of formulations of Si QDs, including "bare" hydrogen-terminated particles, carboxylic acid terminated particles, and micelle-encapsulated particle with a variety of groups on the micelle exterior, at concentrations of up to about 100 μg Si QDs per milliliter of medium. This observation is in contrast to *in vitro* studies using CdTe and CdHgTe QDs, where toxicity effects are observed at much lower concentrations. This demonstrates the enormous potential of Si QDs as biocompatible luminescent probes, and sets the stage for development of multifunctional probes consisting of Si QDs coencapsulated with drugs, pro-drugs, or contrast agents for other imaging modalities. Sailor's group demonstrated that doxorubicin can be incorporated into porous silicon and maintain its chemotherapeutic efficacy.[36] Previous studies demonstrated that systemic levels of encapsulated doxorubicin decrease by 14-fold following injection with targeted PEGylated liposomal doxorubicin, when compared to that of nontargeted liposomal doxorubicin.[49] Efforts are currently underway to further improve the *in vivo* targeting and imaging of QD based probes, which includes improving the QY along with encapsulation of single Si nanocrystals for applications where smaller constructs are needed (e.g., more rapid SLN mapping), narrowing the emission spectrum *via* size-selection, direct conjugation of individual Si nanocrystals to PEG-maleimide linkers, multivalent targeting, *etc.*

A key question in nanomedicine is whether QDs can be used directly in patients.[38] Use of highly toxic elements in QD formulations, irrespective of dosage, creates public apprehension which limits the potential for use in humans. To maintain the promise of QDs and alleviate their associated toxicity concerns, we have demonstrated that Si is a suitable replacement for other, heavy-metal based NIR-emitting QDs in major biomedical applications: tumor targeting, sentinel lymph node mapping, and multiplex NIR imaging. This can move Si nanocrystals to the forefront of QD research, with relevance not only limited to cancer surgery, diagnosis and therapy, but also extended to a wide range of other biological applications where toxicity concerns can otherwise prevent the potential of QDs from being realized.

MATERIALS AND METHODS

Materials. Silane (SiH_4, Voltaix, electronic grade, 99.999%), hydrofluoric acid (HF, Acros Organic, 48−51%), nitric acid (HNO_3, EMD, 68−70%), ethyl undecylenate (Sigma-Aldrich 95%), and RGD peptides (PCI-3686-PI, Peptides International, Inc.) were used as received if not otherwise noted. All solvents (chloro-

form, HPLC water, methanol) were of reagent grade and were used without further purification.

Synthesis of Silicon Quantum Dots. The nonluminescent silicon nanoparticles were prepared by decomposing silane (SiH_4) *via* high temperature CO_2 laser pyrolysis in an aerosol reactor based on the method developed by Li *et al.*[43,44] These particles were handled in a nitrogen glovebox to avoid oxidation. To produce hydrogen-terminated photoluminescent Si QDs, a modified version of a protocol we previously reported[14] was used. The silicon nanoparticles were dispersed in methanol then etched in a mixture of hydrofluoric acid (48 wt %) and nitric acid (69 wt %) (10/1, v/v) for 2 to 4 min. Typically, 300 mg of silicon nanoparticles were dispersed in 30 mL of methanol by sonication. The silicon-methanol mixture was added to the acid mixture and stirred until the luminescence emission spectrum approached the desired color. At that point, 400 mL of methanol was added to quench the reaction. After washing the etched particles with a water−methanol mixture (3/1, v/v) three times (500 mL, 500 mL, 250 mL) to remove the adsorbed acid, we collected the particles on a poly(vinylidene fluoride) (PVDF) membrane filter (Millipore, hydrophilic Durapore, 0.1 μm pore size). Finally, the membrane was rinsed with pure methanol. The particles were finally sonicated from the membrane into vials containing ethyl undecylenate. All these steps were completed in the glovebox to prevent the oxidation of the Si QDs.

A Rayonet photochemical reactor (Southern New England Ultraviolet Co.) equipped with 16 RPR-2537 Å UV tubes was used to initiate the hydrosilylation reaction. The reaction time required varied substantially depending on the compound being attached to the particles and the particle size. After reaction, a clearer dispersion was obtained. It was drawn through a PTFE syringe filter (pore size 0.45 μm).

Micelle Encapsulation. The functionalized particles were removed from excess solvent by flocculation with a semi polar methanol mixture then centrifugation (10 000 rpm for 1 h). The particles were washed 3 times in methanol and then redispersed in chloroform. The encapsulation procedure previously reported by our group was modified slightly here. In a typical experiment, a 1:20 ratio of Si QD to phospholipid was mixed in chloroform in a 100 mL round-bottom flask. The mixture was sonicated. A Labconco rotary evaporator with a water bath of 37 °C was used to evaporate the solvents. The lipidic film, deposited on the reaction vial, was hydrated with 3−5 mL of HPLC water and subjected to ultrasonication for 10 min using a bath sonicator. The particles were centrifuged for purification. The resulting dispersion was filtered through a 0.2 μm membrane filter and kept at 4 °C for further use.

RGD Conjugation. A 1 mL portion of a maleimide terminated MSiQD was mixed with 0.5 mL of 1.2 mg/mL of a thiolated RGD peptide solution and gently stirred for 40−60 min. Next, the resulting bioconjugate dispersion was further purified using centrifugation at 10 000 rpm for 15 min. The MSiQD-cRGD precipitate was redispersed with 1 mL of HPLC water and kept at 4 °C for further use.

Characterization of the Silicon Quantum Dots. The QD emission spectra were collected using a Fluorolog-3 spectrofluorometer (Jobin Yvon; fluorescence spectra). Fluorescence quantum yields (QYs) of the QD dispersions were determined by comparing the integrated emission from the QDs to rhodamine 6G dye solutions of matched absorbance. High-resolution transmission electron microscopy (HRTEM) images were obtained using a JEOL model JEM 2010 microscope at an acceleration voltage of 200 kV. The specimens were prepared by drop-coating the sample dispersion onto an amorphous carbon-coated 300 mesh copper grid, which was placed on filter paper to absorb excess solvent. Hydrophobic Si QDs were drop cast from chloroform and hydrophilic SiDQs were drop cast from water. The size distribution of the silicon quantum dots was determined by dynamic light scattering (DLS) measurement with a Brookhaven Instruments 90Plus particle size analyzer, with a scattering angle of 90°.

Histological Analysis. MSiQDs at a total dose of 380 mg kg^{-1} were injected into the mice *via* tail vein in the histological study. Liver, spleen, heart, lung, and kidney were removed from the sacrificed mice. Tissues were harvested at different time points including 4 weeks, 6 weeks and 8 weeks after intravenous injection of the MSiQDs, fixed in 10% formalin, embedded in paraffin, sectioned, and stained with hematoxylin and eosin. The histological sections were observed under an optical microscope with different combinations of magnification and objective lens of the microscope. Micrographs of the sections were recorded for comparison.

Cell Viability. For each MTS assay, 24 culture wells (8 sets, each set contains 3 wells) of Panc-1 cell were prepared. Seven sets were treated with different concentration of silicon quantum dots and one set was the control The complete assay was performed thrice, and results were averaged. Various concentrations of micelle-encapsulated silicon quantum dots ranging from 1 to 32 μg/mL, were added to each well and subsequently incubated with the cells for 24 and 48 h at 37 °C under 5% CO_2. As described in the literature, the absorbance of formazan (produced by the cleavage of MTS by dehydrogenases in living cells) is directly proportional to the number of live cells. After the incubation, 150 μL of MTS reagent was then added to each well and well mixed. The absorbance of the mixtures at 490 nm was measured. The cell viability was calculated as the ratio of the absorbance of the sample well to that of the control well and expressed as a percentage.

Small Animal Imaging Studies. Four to five week old nude female mice were purchased from Harlan Sprague−Dawley Inc. The animal housing area was maintained at 24 °C with a 12 h light/dark cycle, and animals were fed ad libitum with water and standard laboratory chow. Animal experiments were performed in compliance with guidelines set by the University at Buffalo (SUNY) IACUC. All animals were acclimated to the animal facility for at least 48 h prior to experimentation. Tumor model animals were generated by the subcutaneous inoculation (2−3 million cells/100 μL of media) of human pancreatic cancer cell-line Panc-1 (ATCC NO: CRL-1469) in the shoulder of animals using a 1 mL syringe with a 25G needle. After tumor growth to a palpable size, the mice were administered functionalized MSiQD by tail vein injection and anesthetized with isoflurane at various time points postinjection. The sedated animals were then imaged using the Maestro *in vivo* optical imaging system (CRI, Inc., Woburn, MA). Mice were divided into experimental and control groups in the tumor imaging studies.

Generation of Orthotopic Xenografts. Orthotopic pancreatic cancer xenografts were generated by surgical orthotopic implantation under the pancreatic capsule, as we have previously described.[47] Imaging of the primary tumors was performed 4 weeks postimplantation.

Acknowledgment. This study was supported by grants from the NSF IGERT, NCI RO1CA119397, the John R. Oishei Foundation, the University at Buffalo Gerald Sterbutzel Fund, and the University at Buffalo Interdisciplinary Research and Creative Activities Fund.

Supporting Information Available: (1) Hydrodynamic diameter distributions (from dynamic light scattering) of micelle encapsulated silicon, (2) absorbance spectra of silicon particles of varying size, (3) cytotoxicity data for different silicon nanoparticle formulations, (4) cellular imaging with the MSiQDs, and (5) biodistribution information. This material is available free of charge *via* the Internet at http://pubs.acs.org.

REFERENCES AND NOTES

1. Dubertret, B.; Skourides, P.; Norris, D. J.; Noireaux, V.; Brivanlou, A. H.; Libchaber, A. In Vivo Imaging of Quantum Dots Encapsulated in Phospholipid Micelles. *Science* **2002**, *298*, 1759–1762.
2. Michalet, X.; Pinaud, F. F.; Bentolila, L. A.; Tsay, J. M.; Doose, S.; Li, J. J.; Sundaresan, G.; Wu, A. M.; Gambhir, S. S.; Weiss, S. Quantum Dots for Live Cells, In Vivo Imaging, and Diagnostics. *Science* **2005**, *307*, 538–544.
3. Prasad, P. N., *Biophotonics*: Wiley-Interscience: Hoboken, NJ, 2003.
4. Prasad, P. N., *Nanophotonics*: Wiley-Interscience: Hoboken, NJ, 2004.

5. Fu, A.; Gu, W.; Larabell, C.; Alivisatos, A. P. Semiconductor Nanocrystals for Biological Imaging. *Curr. Opin. Neurobiol.* **2005**, *15*, 568–575.
6. Gao, X.; Cui, Y.; Levenson, R. M.; Chung, L. W. K.; Nie, S. In Vivo Cancer Targeting and Imaging with Semiconductor Quantum Dots. *Nat. Biotechnol.* **2004**, *22*, 969–976.
7. Derfus, A. M.; Chan, W. C. W.; Bhatia, S. N. Probing the Cytotoxicity of Semiconductor Quantum Dots. *Nano Lett.* **2004**, *4*, 11–18.
8. Ron, H. A Toxicologic Review of Quantum Dots: Toxicity Depends on Physicochemical and Environmental Factors. *Environ. Health Perspect.* **2006**, *114*, 165–172.
9. Kloepfer, J. A.; Mielke, R. E.; Wong, M. S.; Nealson, K. H.; Stucky, G.; Nadeau, J. L. Quantum Dots as Strain- and Metabolism-Specific Microbiological Labels. *Appl. Environ. Microbiol.* **2003**, *69*, 4205–4213.
10. Smith, A. M.; Duan, H.; Mohs, A. M.; Nie, S. Bioconjugated Quantum Dots for *In Vivo* molecular and cellular imaging. *Adv. Drug Delivery Rev.* **2008**, *60*, 1226–1240.
11. Zimmer, J. P.; Kim, S. W.; Ohnishi, S.; Tanaka, E.; Frangioni, J. V.; Bawendi, M. G. Size Series of Small Indium Arsenide-Zinc Selenide Core-Shell Nanocrystals and Their Application to In Vivo Imaging. *J. Am. Chem. Soc.* **2006**, *128*, 2526–2527.
12. Pons, T.; Pic, E.; Lequeux, N.; Cassette, E.; Bezdetnaya, L.; Guillemin, F.; Marchal, F.; Dubertret, B. Cadmium-Free $CuInS_2$/ZnS Quantum Dots for Sentinel Lymph Node Imaging with Reduced Toxicity. *ACS Nano* **2010**, *4*, 2531–2538.
13. English, D. S.; Pell, L. E.; Yu, Z.; Barbara, P. F.; Korgel, B. A. Size Tunable Visible Luminescence from Individual Organic Monolayer Stabilized Silicon Nanocrystal Quantum Dots. *Nano Lett.* **2002**, *2*, 681–685.
14. Hua, F.; Swihart, M. T.; Ruckenstein, E. Efficient Surface Grafting of Luminescent Silicon Quantum Dots by Photoinitiated Hydrosilylation. *Langmuir* **2005**, *21*, 6054–6062.
15. O'Farrell, N.; Houlton, A.; Horrocks, B. R. Silicon Nanoparticles: Applications in Cell Biology and Medicine. *Int. J. Nanomed.* **2006**, *1*, 451–472.
16. Sato, S.; Swihart, M. T. Propionic-Acid Terminated Silicon Nanoparticles: Synthesis and Optical Characterization. *Chem. Mater.* **2006**, *18*, 4083–4088.
17. Swihart, M. T. Silicon Nanoparticles for Biophotonics. In *Nanotechnology in Biology and Medicine: Methods, Devices, and Applications*; Dinh, T. V., Ed.; CRC Press: Boca Raton, FL, 2007.
18. Tilley, R. D.; Yamamoto, K. The Microemulsion Synthesis of Hydrophobic and Hydrophilic Silicon Nanocrystals. *Adv. Mater.* **2006**, *18*, 2053–2056.
19. Tinsley-Bown, A. M.; Canham, L. T.; Hollings, M.; Anderson, M. H.; Reeves, C. L.; Cox, T. I.; Nicklin, S.; Squirrell, D. J.; Perkins, E.; Hutchinson, A.; Sailor, M. J.; Wun, A. Tuning the Pore Size and Surface Chemistry of Porous Silicon for Immunoassays. *Phys. Status Solidi A* **2000**, *182*, 547–553.
20. Wang, L.; Reipa, V.; Blasic, J. Silicon Nanoparticles as a Luminescent Label to DNA. *Bioconjugate Chem.* **2004**, *15*, 409–412.
21. Zhang, X.; Neiner, D.; Wang, S.; Louie, A. Y.; Kauzlarich, S. M. A New Solution Route to Hydrogen-Terminated Silicon Nanoparticles: Synthesis, Functionalization and Water Stability. *Nanotechnology* **2007**, *18*, 095601.
22. Baldwin, R. K.; Pettigrew, K. A.; Garno, J. C.; Power, P. P.; Liu, G. y.; Kauzlarich, S. M. Room Temperature Solution Synthesis of Alkyl-Capped Tetrahedral Shaped Silicon Nanocrystals. *J. Am. Chem. Soc.* **2002**, *124*, 1150–1151.
23. Bley, R. A.; Kauzlarich, S. M. A Low-Temperature Solution Phase Route for the Synthesis of Silicon Nanoclusters. *J. Am. Chem. Soc.* **1996**, *118*, 12461–12462.
24. Heath, J. R. A Liquid-Solution-Phase Synthesis of Crystalline Silicon. *Science* **1992**, *258*, 1131–1133.
25. Carlisle, J. A.; Dongol, M.; Germanenko, I. N.; Pithawalla, Y. B.; El-Shall, M. S. Evidence for Changes in the Electronic and Photoluminescence Properties of Surface-oxidized Silicon Nanocrystals Induced by Shrinking the Size of the Silicon Core. *Chem. Phys. Lett.* **2000**, *326*, 335–340.
26. Hessel, C. M.; Henderson, E. J.; Veinot, J. G. C. Hydrogen Silsesquioxane: A Molecular Precursor for Nanocrystalline Si-SiO_2 Composites and Freestanding Hydride-Surface-Terminated Silicon Nanoparticles. *Chem. Mater.* **2006**, *18*, 6139–6146.
27. Mangolini, L.; Thimsen, E.; Kortshagen, U. High-Yield Plasma Synthesis of Luminescent Silicon Nanocrystals. *Nano Lett.* **2005**, *5*, 655–659.
28. Orii, T.; Hirasawa, M.; Seto, T. Tunable, Narrow-Band Light Emission From Size-selected Si Nanoparticles Produced by Pulsed-laser Ablation. *Appl. Phys. Lett.* **2003**, *83*, 3395.
29. Betty, C. A. Porous Silicon: A Resourceful Material for Nanotechnology. *Recent Pat. Nanotechnol.* **2008**, *2*, 128–136.
30. Hua, F. J.; Erogbogbo, F.; Swihart, M. T.; Ruckenstein, E. Organically Capped Silicon Nanoparticles with Blue Photoluminescence Prepared by Hydrosilylation Followed By Oxidation. *Langmuir* **2006**, *22*, 4363–4370.
31. Mangolini, L.; Jurbergs, D.; Rogojina, E.; Kortshagen, U. High Efficiency Photoluminescence From Silicon Nanocrystals Prepared by Plasma Synthesis and Organic Surface Passivation. *Phys. Status Solidi C* **2006**, *3*, 3975–3978.
32. He, G. S.; Zheng, Q.; Yong, K.-T.; Erogbogbo, F.; Swihart, M. T.; Prasad, P. N. Two- and Three-Photon Absorption and Frequency Upconverted Emission of Silicon Quantum Dots. *Nano Lett.* **2008**, *8*, 2688–2692.
33. Canham, L. T. Nanoscale Semiconducting Silicon as a Nutritional Food Additive. *Nanotechnology* **2007**, *18*, 185704.
34. Fujioka, K.; Hiruoka, M.; Sato, K.; Manabe, N.; Miyasaka, R.; Hanada, S.; Hoshino, A.; Tilley, R. D.; Manome, Y.; Hirakuri, K.; Yamamoto, K. Luminescent Passive-Oxidized Silicon Quantum Dots as Biological Staining Labels and Their Cytotoxicity Effects at High Concentration. *Nanotechnology* **2008**, *19*, 415102.
35. Canham, L. T. Bioactive Silicon Structure Fabrication Through Nanoetching Techniques. *Adv. Mater.* **1995**, *7*, 1033–1037.
36. Park, J.-H.; Gu, L.; von Maltzahn, G.; Ruoslahti, E.; Bhatia, S. N.; Sailor, M. J. Biodegradable Luminescent Porous Silicon Nanoparticles for *In Vivo* Applications. *Nat. Mater.* **2009**, *8*, 331–336.
37. Soltesz, E. G.; Kim, S.; Laurence, R. G.; DeGrand, A. M.; Parungo, C. P.; Dor, D. M.; Cohn, L. H.; Bawendi, M. G.; Frangioni, J. V.; Mihaljevic, T. Intraoperative Sentinel Lymph Node Mapping of the Lung Using Near-Infrared Fluorescent Quantum Dots. *Ann. Thorac. Surg.* **2005**, *79*, 269–277.
38. Cai, W.; Shin, D. W.; Chen, K.; Gheysens, O.; Cao, Q.; Wang, S. X.; Gambhir, S. S.; Chen, X. Peptide-Labeled Near-Infrared Quantum Dots for Imaging Tumor Vasculature in Living Subjects. *Nano Lett.* **2006**, *6*, 669–676.
39. Stroh, M.; Zimmer, J. P.; Duda, D. G.; Levchenko, T. S.; Cohen, K. S.; Brown, E. B.; Scadden, D. T.; Torchilin, V. P.; Bawendi, M. G.; Fukumura, D.; Jain, R. K. Quantum Dots Spectrally Distinguish Multiple Species Within the Tumor Milieu *In vivo*. *Nat. Med.* **2005**, *11*, 678–682.
40. Alsharif, N. H.; Berger, C. E. M.; Varanasi, S. S.; Chao, Y.; Horrocks, B. R.; Datta, H. K. Alkyl-Capped Silicon Nanocrystals Lack Cytotoxicity and have Enhanced Intracellular Accumulation in Malignant Cells via Cholesterol-Dependent Endocytosis. *Small* **2009**, *5*, 221–228.
41. Choi, J.; Zhang, Q.; Reipa, V.; Wang, N. S.; Stratmeyer, M. E.; Hitchins, V. M.; Goering, P. L. Comparison of cytotoxic and inflammatory responses of photoluminescent silicon nanoparticles with silicon micron-sized particles in RAW 264.7 macrophages. *J. Appl. Toxicol.* **2009**, *29*, 52–60.
42. Ruizendaal, L.; Bhattacharjee, S.; Pournazari, K.; Rosso-Vasic, M.; de Haan, L. H. J.; Alink, G. M.; Marcelis, A. T. M.;

Zuilhof, H. Synthesis and cytotoxicity of silicon nanoparticles with covalently attached organic monolayers. *Nanotoxicology* **2009**, *3*, 339–347.
43. Li, X.; He, Y.; Swihart, M. T. Surface Functionalization of Silicon Nanoparticles Produced by Laser-Driven Pyrolysis of Silane followed by HF-HNO_3 Etching. *Langmuir* **2004**, *20*, 4720–4727.
44. Li, X. G.; He, Y. Q.; Talukdar, S. S.; Swihart, M. T. Process for Preparing Macroscopic Quantities of Brightly Photoluminescent Silicon Nanoparticles with Emission Spanning the Visible Spectrum. *Langmuir* **2003**, *19*, 8490–8496.
45. Erogbogbo, F.; Yong, K.-T.; Roy, I.; Xu, G.; Prasad, P. N.; Swihart, M. T. Biocompatible Luminescent Silicon Quantum Dots for Imaging of Cancer Cells. *ACS Nano* **2008**, *2*, 873–878.
46. Kim, S.; Lim, Y. T.; Soltesz, E. G.; De Grand, A. M.; Lee, J.; Nakayama, A.; Parker, J. A.; Mihaljevic, T.; Laurence, R. G.; Dor, D. M.; Cohn, L. H.; Bawendi, M. G.; Frangioni, J. V. Near-Infrared Fluorescent Type II Quantum Dots for Sentinel Lymph Node Mapping. *Nat. Biotechnol.* **2004**, *22*, 93–97.
47. Feldmann, G.; Fendrich, V.; McGovern, K.; Bedja, D.; Bisht, S.; Alvarez, H.; Koorstra, J.-B. M.; Habbe, N.; Karikari, C.; Mullendore, M.; Gabrielson, K. L.; Sharma, R.; Matsui, W.; Maitra, A. An Orally Bioavailable Small-molecule Inhibitor of Hedgehog Signaling Inhibits Tumor Initiation and Metastasis in Pancreatic Cancer. *Mol. Cancer Ther.* **2008**, *7*, 2725–2735.
48. Ducongeì, F.; Pons, T.; Pestourie, C.; Heìrin, L.; Theìzeì, B.; Gombert, K.; Mahler, B.; Hinnen, F.; Kühnast, B.; Dolleì, F.; Dubertret, B.; Tavitian, B. Fluorine-18-Labeled Phospholipid Quantum Dot Micelles for *In Vivo* Multimodal Imaging from Whole Body to Cellular Scales. *Bioconjugate Chem.* **2008**, *19*, 1921–1926.
49. Shmeeda, H.; Mak, L.; Tzemach, D.; Astrahan, P.; Tarshish, M.; Gabizon, A. Intracellular Uptake and Intracavitary Targeting of Folate-Conjugated Liposomes in a Mouse Lymphoma Model with Up-regulated Folate Receptors. *Mol. Cancer Ther.* **2006**, *5*, 818–824.